Hindawi
Advances in Materials Science and Engineering
Volume 2024, Article ID 9786960, 1 page
https://doi.org/10.1155/2024/9786960

Retraction

Retracted: Optimizing the Characteristics of the Laser Hardfacing Process Parameters to Maximize the Wear Resistance of Ni-Based Hard-Faced Deposits Using the RSM Technique

Advances in Materials Science and Engineering

Received 23 January 2024; Accepted 23 January 2024; Published 24 January 2024

This article has been retracted by Hindawi following an investigation undertaken by the publisher [1]. This investigation has uncovered evidence of one or more of the following indicators of systematic manipulation of the publication process:

(1) Discrepancies in scope

(2) Discrepancies in the description of the research reported

(3) Discrepancies between the availability of data and the research described

(4) Inappropriate citations

(5) Incoherent, meaningless and/or irrelevant content included in the article

(6) Manipulated or compromised peer review

The presence of these indicators undermines our confidence in the integrity of the article's content and we cannot, therefore, vouch for its reliability. Please note that this notice is intended solely to alert readers that the content of this article is unreliable. We have not investigated whether authors were aware of or involved in the systematic manipulation of the publication process.

Wiley and Hindawi regrets that the usual quality checks did not identify these issues before publication and have since put additional measures in place to safeguard research integrity.

We wish to credit our own Research Integrity and Research Publishing teams and anonymous and named external researchers and research integrity experts for contributing to this investigation.

The corresponding author, as the representative of all authors, has been given the opportunity to register their agreement or disagreement to this retraction. We have kept a record of any response received.

References

[1] S. Gnanasekaran, S. J. S. Chelladurai, T. Ramakrishnan et al., "Optimizing the Characteristics of the Laser Hardfacing Process Parameters to Maximize the Wear Resistance of Ni-Based Hard-Faced Deposits Using the RSM Technique," *Advances in Materials Science and Engineering*, vol. 2021, Article ID 3665631, 15 pages, 2021.

Hindawi
Advances in Materials Science and Engineering
Volume 2021, Article ID 3665631, 15 pages
https://doi.org/10.1155/2021/3665631

Research Article

Optimizing the Characteristics of the Laser Hardfacing Process Parameters to Maximize the Wear Resistance of Ni-Based Hard-Faced Deposits Using the RSM Technique

S. Gnanasekaran,[1] **Samson Jerold Samuel Chelladurai**,[2] **T. Ramakrishnan**,[3] **S Sivananthan**,[4] **G. Padmanaban**,[5] **Ramesh Arthanari**,[6] **and V. Balasubramanian**[5]

[1]*Department of Mechanical Engineering, Sri Shakthi Institute of Engineering and Technology, Chinniyampalayam, Coimbatore, Tamil Nadu, India*
[2]*Department of Mechanical Engineering, Sri Krishna College of Engineering and Technology, Coimbatore, Tamilnadu, India*
[3]*Department of Mechanical Engineering, Sri Eshwar College of Engineering, Coimbatore, Tamilnadu, India*
[4]*Department of Mechanical Engineering, K. Ramakrishnan College of Engineering, Tamilnadu, India*
[5]*Centre for Materials Joining & Research (CEMAJOR), Department of Manufacturing Engineering, Annamalai University, Annamalainagar, Tamil Nadu, India*
[6]*Department of Mechanical Engineering, Chennai Institute of Technology, Tamil Nadu, India*

Correspondence should be addressed to Samson Jerold Samuel Chelladurai; samsonjeroldsamuel@skcet.ac.in

Received 5 August 2021; Revised 7 October 2021; Accepted 18 October 2021; Published 1 November 2021

Academic Editor: Angela De Bonis

The nickel-based Colmonoy-5 hardfacing alloy is used to hard-face 316LN austenitic stainless steel components in fast reactors. The nominal composition (in wt%) was listed as follows: 0.01 C, 0.49 Si, 0.87 Mn, 17.09 Cr, 14.04 Ni, 2.56 Mo, 0.14 N, and balance Fe. Hardfacing is a technique of applying hard and wear-resistant materials to substrates that need abrasion resistance. The thickness of hardfacing deposit varies between 0.8 mm and 2 mm based on parameter combinations. In this study, laser hardfacing process parameters including laser power, powder feed rate, travel speed, and defocusing distance were optimized to reduce weight loss of laser hard-faced Ni-based deposit. The tribological characteristics of reactor-grade NiCr-B hard-faced deposits were investigated. The RSM technique was used to identify the most important control variables resulting in the least weight loss of the nickel-based alloy placed on AISI 316LN austenitic stainless steel. Statistical techniques like DoE and ANOVA are utilized. Changing the laser settings may efficiently track the weight loss of laser hard-faced nickel alloy surfaces. These are created using the response surface technique. The deposit produced with a laser power of 1314 W, powder feed rate of 9 g/min, travel speed of 366 mm/min, and defocusing distance of 32 mm had the lowest weight loss of 16.4 mg. Based on the F value, the powder feed rate is the major influencing factor to predict the hardness followed by power, travel speed, and defocusing distance.

1. Introduction

Prototype Fast Breeder Reactor (PFBR) is a 500 MWe pool type sodium-cooled nuclear reactor having two separate sodium circuits with the intermediate heat exchanger (IHX) providing thermal contact between the primary pool and the secondary circuit. The secondary sodium circuits transfer heat from the IHX to the steam generator (SG), the steam from which drives the conventional steam turbines. The minimum sodium temperature in the primary pool during normal operation is 400°C, while the mean above-core temperature is 550°C. The minimum and maximum sodium temperatures in the secondary circuit are 355 and 525°C, respectively. The steam temperature is 490°C at 16.6 MPa pressure. Austenitic stainless steel (SS) is the major material of construction for PFBR. The Main Vessel, Inner Vessel, GridPlate, and Primary Piping, etc., whose service temperatures are above 427°C, are made of numerous austenitic

stainless steel components that come into touch with flowing liquid sodium at temperatures of up to 823 K. Due to the fact that flowing liquid sodium dissolves the oxide layer that typically forms on metallic surfaces, prolonged static contact between mating surfaces may result in self-welding. When components move in relation to one another, galling occurs. By hardfacing these components with nickel or cobalt-based alloy powders, self-welding and galling resistance are increased. While alloys based on Co are extensively used as high-temperature hardfacing materials [1–4], induced radioactivity from transmuted Co^{60} isotopes is generated in a nuclear reactor environment [5, 6]. Colmonoy grades, because of their high chromium and boron content, may be used in place of Co-based Stellite alloys for abrasive and adhesive wear resistance. Colmonoy alloys are tougher than Stellite alloys because they include chromium carbides and borides in the deposit, while Stellite contains just carbide precipitates [7, 8].

Wear resistance is a material's mechanical characteristic that allows it to withstand surface damage during sliding contact [9]. The chemical, physical, and mechanical characteristics of wear-generated scars vary throughout tribological testing. Changes in wear scar morphology may affect frictional force. Wear mechanisms on steel-based alloys are classified as adhesive, abrasive, oxidation, and plastic extrusion [10, 11]. In general, material wear resistance is inversely linked to hardness. This deposit's superior wear resistance to stainless steel extends the life of FBR components. Despite its improved mechanical characteristics, this alloy's friction and wear as a function of sliding distance remain unknown. Hardfacing process factors affect deposit quality. Few studies have examined the impact of laser process parameters on wear characteristics [5]. The softer dilution zone frequently exceeds the ultimate required hard-faced deposit thickness in conventional welding techniques like gas tungsten arc welding (GTAW) and plasma transferred arc welding (PTAW). So, the more flexible laser hardfacing method was selected to minimize the dilution zone by adjusting the deposition settings.

Zhang et al. [12] used a CO_2 laser to clad 316 L austenitic stainless steel with Colmonoy 6 powder. A reduced friction coefficient and higher wear resistance after laser cladding were observed, indicating that the laser cladding layer plays a significant role in wear resistance. Laser cladding microstructures include eutectic, boride, and carbide. Hemmati et al. [13] observed that specimens with laser and PTA hardfacing had friction values of 0.42–0.48 and 0.51–0.58. Laser and PTA hardfacing both lose mass (7 and 380 mg). Laser hardfacing has a lower friction coefficient and a lower wear mass loss than PTA hardfacing. Laser cladding and wear testing of nickel base hardfacing materials have process parameter effects on ASTM [14]. They found that two laser cladding samples with differing travel speeds had very distinct wear processes. The laser cladding process may adapt the hardfacing material quality to the tribology circumstances and applications by varying the process parameters.

As the process facts have not been revealed yet, selecting process parameters for nickel-based alloys is challenging. A many-factor analysis is a set of mathematical and statistical methods used to model and analyze situations where the goal is to maximize the responses [15]. RSM reduced experimentation and improved process parameters for wear resistance (minimum weight loss). The hardfacing process settings are known to affect the deposits' mechanical and wear resistance. There is no literature available in optimizing the laser hardfacing parameters to attain maximum hardness on nickel-based hard-faced deposit on 316 LN austenitic stainless steel. Hence, in this study, an attempt has been made to optimize the important laser hardfacing parameters to attain maximum hardness in nickel-based hard-faced deposits on 316 LN austenitic stainless steel by RSM.

2. Materials and Methods

The current study's goals were designed as shown in the flow chart (Figure 1).

2.1. Identifying Important Laser Hardfacing Parameters. Choosing variables for the process under study is a first step in designing experiments. Many factors in laser hardfacing have been identified as possibly influencing the deposit's characteristics. It is not feasible to manage all potential parameter changes economically (time) and theoretically (parameter dependency). The following process parameters have been identified as having a greater impact on deposit characteristics: laser power (P), powder feed rate (F), travel speed (T), and defocusing distance (D). All of these factors affect the melting and flattening of powder particles and, therefore, the deposit properties of nickel-based hardfacing.

2.2. Feasible Working Range of Laser Hardfacing Parameters. To determine the possible working limits of laser hardfacing parameters, trial runs were conducted using a 12 mm thick 316 LN austenitic stainless steel plate and nickel-based alloy powder. The experimental tests were conducted using various combinations of factors. This was accomplished by varying the value of any one of the variables from lowest to highest while keeping the other parameters constant (Table 1). Macrostructure was used to determine the practical operating limits of various parameters (cross section of the deposits). The parameter level that produces a deposit with a smooth appearance devoid of visible macrolevel flaws such as fracture and pores was chosen as the parameter's practical working limit. Table 2 lists the selected levels of the specified process parameters, along with their units and notations.

2.3. Developing the Experimental Design Matrix. Taking into account the aforementioned circumstances, the parameter limitations were set so that flawless laser hard-faced deposits could be created. A second-order central composite rotatable design was determined to be the most effective tool in RSM for establishing the empirical connection of the response surface with the least number of trials [16]. To establish an empirical connection, four variables, five levels, and a core composite design matrix were used. The most common response surface technique design is the central

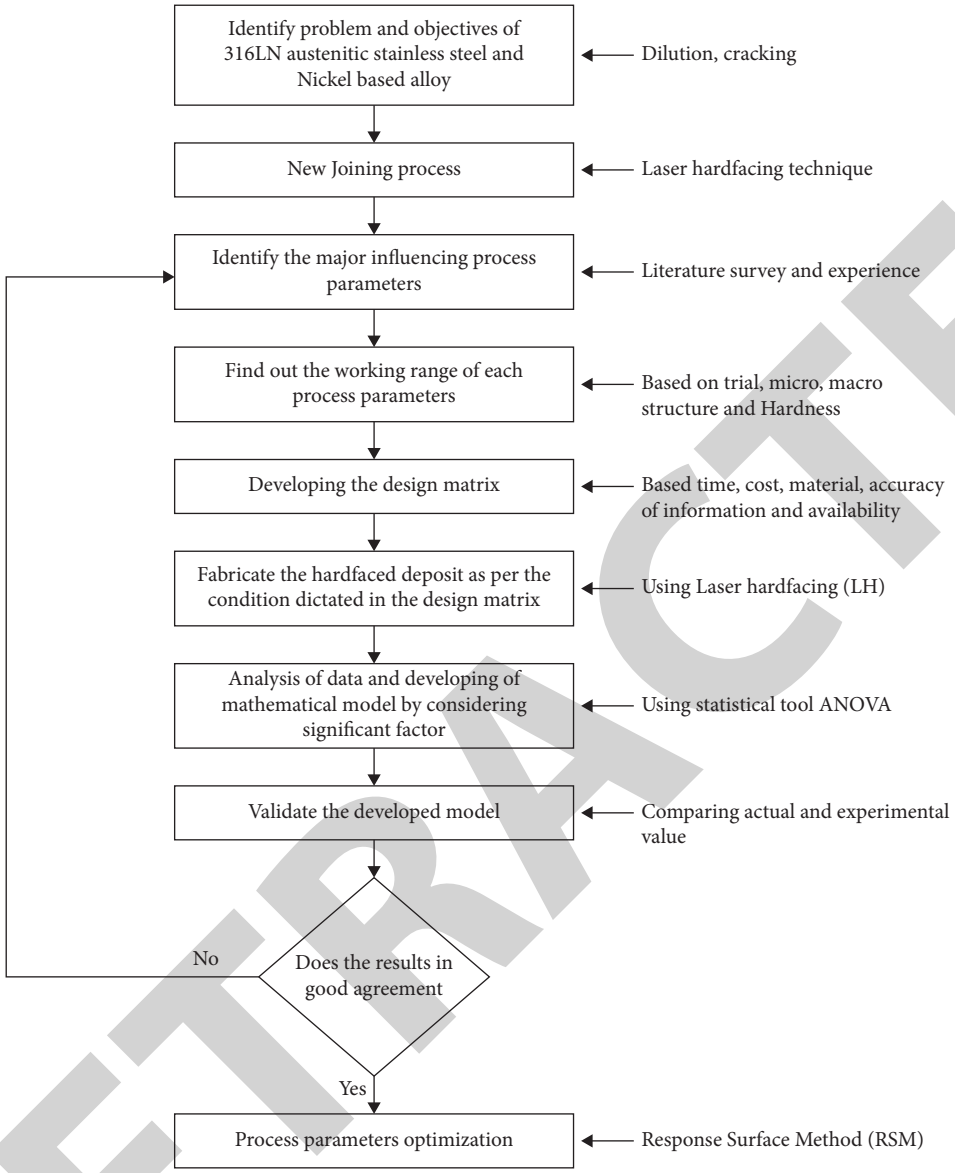

Figure 1: Flow chart for process optimization.

Table 1: Fixing the working range of laser hardfacing macrostructure analysis.

S. no.	Process parameters	Parameter range	Macrograph	Name of the defect
1	Laser power (P)	$P > 1900$ W	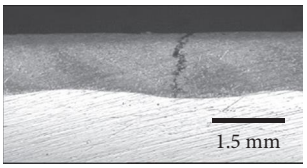	Crack and high dilution
		$P < 1100$ W	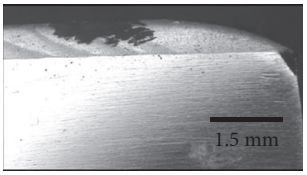	Pores and escaping of powder

Table 1: Continued.

S. no.	Process parameters	Parameter range	Macrograph	Name of the defect
2	Powder feed rate (F)	$F > 11$ g/min	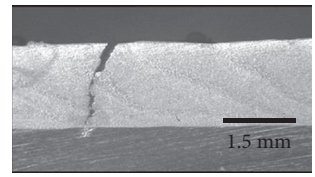	Cracks
		$F < 3$ g/min	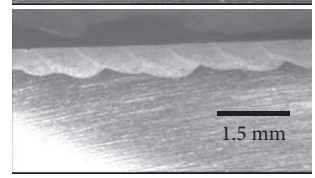	High depth of penetration and high dilution
3	Travel speed (T)	$T > 500$ mm/min	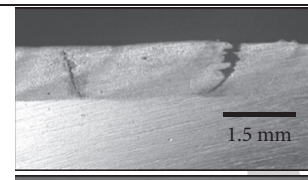	Cracks
		$T < 300$ mm/min	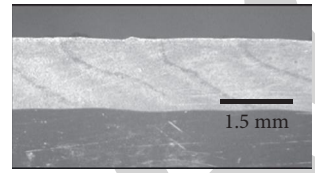	Excess bead height
4	Defocusing distance (D)	$D > 37$ mm	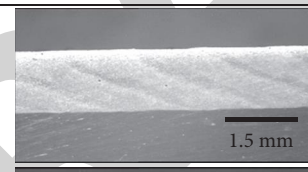	Poor bonding
		$D < 17$ mm	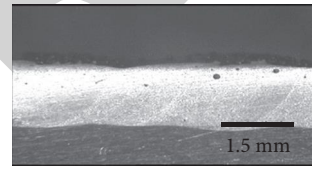	Presence of pores

Table 2: Laser hard-faced processessing parameters and their working range.

S. no.	Factor	Notation	Levels				
			−2	−1	0	1	2
1	Laser power (W)	P	1100	1300	1500	1700	1900
2	Powder feed rate (g/min)	F	3	5	7	9	11
3	Travel speed (mm/min)	T	300	350	400	450	500
4	Defocusing distance (mm)	D	17	22	27	32	37

composite design, which includes three sets of design points: factorial, axial or star, and center. The primary composite design's structure allows for successive experimentation, which is noteworthy. Table 3 displays the design matrix's coded conditions. The design matrix has 30 coded conditions, including 16 four-factor factorial points, 8 star points, and 6 center points.

The star points are formed by combining each process variable's lowest (−2) or highest (+2) level with the other 8 intermediate level variables. In this manner, the 30 experimental conditions enabled estimating the variables' linear, quadratic, and two-way interaction impacts on microhardness and weight loss of laser hard-faced nickel-based deposits. Making such a matrix was previously discussed [17]. The upper and lower values of the variables are labeled as +2 and −2 for ease of collecting and processing experimental results.

2.4. Developing Empirical Relationships. For example, the hardness of the deposit is a function of power (P), powder feed rate (F), travel speed (T), and defocusing distance (D).

$$f = \text{responses}(P, F, T, D). \quad (1)$$

Table 3: Design matrix and experimental results.

Ex no.	Coded value				Actual value				Responses	
	P	F	T	D	P (W)	F (g/m)	T (mm/min)	D (mm)	Microhardness (HV)	Weight loss (mg)
1	−1	−1	−1	−1	1300	5	350	22	573	32.2
2	1	−1	−1	−1	1700	5	350	22	475	41.4
3	−1	1	−1	−1	1300	9	350	22	778	18.3
4	1	1	−1	−1	1700	9	350	22	603	31.3
5	−1	−1	1	−1	1300	5	450	22	475	39
6	1	−1	1	−1	1700	5	450	22	574	29.1
7	−1	1	1	−1	1300	9	450	22	794	25
8	1	1	1	−1	1700	9	450	22	703	18.2
9	−1	−1	−1	1	1300	5	350	32	743	23.8
10	1	−1	−1	1	1700	5	350	32	568	32.8
11	−1	1	−1	1	1300	9	350	32	820	16.4
12	1	1	−1	1	1700	9	350	32	602	32.2
13	−1	−1	1	1	1300	5	450	32	545	36.2
14	1	−1	1	1	1700	5	450	32	581	27.9
15	−1	1	1	1	1300	9	450	32	680	26.8
16	1	1	1	1	1700	9	450	32	648	24.9
17	−2	0	0	0	1100	7	400	27	727	26.2
18	2	0	0	0	1900	7	400	27	551	31.7
19	0	−2	0	0	1500	3	400	27	487	36.8
20	0	2	0	0	1500	11	400	27	770	19.8
21	0	0	−2	0	1500	7	300	27	799	27.7
22	0	0	2	0	1500	7	500	27	721	29.8
23	0	0	0	−2	1500	7	400	17	575	30.4
24	0	0	0	2	1500	7	400	37	681	25
25	0	0	0	0	1500	7	400	27	769	28.7
26	0	0	0	0	1500	7	400	27	766	27.9
27	0	0	0	0	1500	7	400	27	769	28.7
28	0	0	0	0	1500	7	400	27	770	27.9
29	0	0	0	0	1500	7	400	27	766	27.8
30	0	0	0	0	1500	7	400	27	766	27.7

The second-order polynomial (regression) equation for the response surface Y is

$$Y = b_0 + \sum b_i X_i + \sum b_i X_{i2} + \sum b_{ij} X_i X_j. \quad (2)$$

Selected polynomial could be expressed as

$$\begin{aligned} H = {} & b0 + b1(P) + b2(F) + b3(T) + b4(D) + b12(PF) \\ & + b13(PT) + b14(PD) + b23(FT) + b24(FD) \\ & + b11(P2) + b22(F2) + b33(T2) + b44(D2). \end{aligned} \quad (3)$$

B1, B2, B3, and B44 are linear interactions and factor square terms. The coefficient was estimated with 95% confidence using Design-Expert 7 software. The t-test and P values of each coefficient were computed. Model terms are significant when "Probe > F" is less than 0.05.

The important terms are P^2, F^2, and D^2. The final empirical connection of laser hard-faced deposit of colmonoy-5 alloy was developed utilizing just these coefficient.:

$$\begin{aligned} \text{hardness of the deposit}(H) = {} & \left(\begin{array}{c} 772.50 - 41.92(P) + 69.17(F) - 13.25(T) + 17.67(D) - 23.62(P*F) \\ +42.38(P*T) - 7.75(P*D) + 12.88(F*T) - 29.25(F*D) \\ -24.75\ (T*D) - 38.17(P2) - 40.79(F2) - 7.92(T2) - 40.92(D2) \end{array} \right) \text{HV}. \\ \text{weight loss} = {} & \left(\begin{array}{c} -83.403 + 0.1353(P) - 10.642(F) + 0.5610(T) - 4.410(D) \\ +3.140E-3(P*F) - 4.618E-4(P*T) - 7.75(P*D) - 3.312E-3(F*T) \\ +0.1781(F*D) + 5.625-3(T*D) + 6.171E-6\left(P^2\right) + 0.0210\left(F^2\right) + 3.750E-6\left(T^2\right) - 2.625E-3\left(D^2\right) \end{array} \right) \text{mg}. \end{aligned} \quad (4)$$

2.5. Checking Adequacy of the Developed Relationships. The established empirical connections were tested using ANOVA. In this study, 95% confidence was sought. The connection is sufficient. The estimated F ratio of the generated model should not exceed the standard tabulated F ratio, and the calculated R ratio should surpass the standard tabulated R ratio for a specified degree of confidence. The model is determined to be sufficient. The likelihood > F in Tables 4 and 5 is less than 0.05, indicating that the empirical connections are significant. The lack of fit was not substantial for all empirical connections. The model is sufficient if the computed F ratio of the generated relationship does not exceed the predicted F ratio for a given degree of confidence. Fisher's F-test with a low probability value shows the regression model's high significance. The determination coefficient measures the model's fit (R^2). The coefficient of determination was determined to be 0.99, meaning that 99 percent of the experimental results agree with the model's predictions. R^2 should always be 0-1. A statistically sound model has an R^2 near 1.0.

Then, we reconstruct the phrase using important terms. Adj. $R^2 = 0.981$ also shows the model's high relevance. To put it another way, the model could explain 82.2 percent of the variability in prediction. This is in line with the Adj. R^2 of 0.952. The coefficient of variation is 2.17, indicating that the difference between experimental and anticipated values is small. A signal-to-noise ratio higher than 4 is ideal. With a ratio of 34.47, the signal is sufficient. To utilize this model, go here. The correlation graph in Figures 2(a) and 2(b) illustrates anticipated and actual hardness of laser hard-faced deposit, indicating minimal variation between the two. Figure 3 shows the microhardness and weight loss of all thirty experiments with an error bar. Table 6 shows the ANOVA test result for weight reduction. The table shows that the created statistical model met the 95% confidence level. In this case, the predicted and experimental values were compared using R2. The "R^2" score for the above-developed model shows a strong correlation between estimated and experimental values. As demonstrated in Figures 2(a) and 2(b), the established empirical connections may be successfully utilized for prediction.

2.6. Verification of Developed Empirical Relationships. It is critical to check that the empirical connections established satisfy the requirements and the results are accurate. This is the procedure of validation. For validation, four alternative laser hardfacing process parameter combinations were used that were not specified in the design matrix (Table 3). Tables 6 and 7 show the experimental and anticipated findings. The anticipated values of microhardness and weight loss match well with the actual data, with only small deviations (5%).

3. Results and Discussion

3.1. Perturbation Plots. By replacing process parameter values in the coded form, the empirical connections may be utilized to anticipate responses. The primary and interaction impacts of process factors on deposit characteristics were calculated and shown as perturbation plots in Figures 4 and 5. The perturbation plot is a diagrammatic depiction of the response surface. The perturbation plot compares the impacts of all variables in the RSM design space.

In response to surface designs, the perturbation plot illustrates how the response varies as each component moves away from the reference point. The default reference point in Design-Expert software is in the design space (the coded zero level of each factor). A high slope or curve in a factor indicates a sensitive reaction. A generally flat line indicates insensitivity to change [18]. Using F values, one may also evaluate the main variables that have significant and small impacts on the answers. According to the F value analysis, the most important variables influencing the reactions are input power, stand-off distance, and powder feed rate. Figures 4–5 indicate a strong impact that agrees well with the anticipated model F values.

Figure 4 shows a perturbation plot for the deposit hardness response. Figure 4 shows the change of hardness when each laser hardfacing parameter travels away from the reference point, while all other parameters remain constant. The experiment's design places the reference point at the design space's center. The perturbation and response surface graphs show that when hardness rises, defocusing distance climbs to a point and then declines. Insufficient energy or low heat input causes powders and unmelted partials to escape from deposits. Laser power and travel speed reduce hardness. The increased heat input may enhance penetration depth and diluting of deposits [19].

3.2. Process Optimization. The RSM was utilized to improve the laser hardfacing parameters in this research. RSM is a set of mathematical and statistical methods used for planning experiments, building mathematical models, determining optimum input parameter combinations, and displaying results visually [20]. As illustrated in Figure 6, two parameters in the midway tier and two parameters in the X-axis and Y-axis were used to construct surface and contour plots that indicate potential factor independence. In the design realm, contour plots assist us to anticipate reaction [21]. On the response plot, the apex represents maximal hardness.

To categorize a stationary point, we determine if it is a minimum, maximum, or saddle point using a contour plot. A contour plot is important in learning response surfaces. It is noticeable that as the powder feed rate rises, so does the defocusing distance and hardness. Three-dimensional diagrams are drawn for a specific processing condition to learn more about how process factors affect hardness. Surface and contour graphs for each process parameter are shown in Figure 6. Figure 6(a) shows that when process parameters like laser power and powder feed rate rise, the hardness decreases. Dilution and microstructure affect hardness. Laser power dissolves powder, and heat melts the substrate. As the laser intensity increases, more substrate material melts.

The deposit dilution may influence the hardness variation in laser hard-faced samples. Higher dilution reduces hardness. Increasing power (constant F, T, D) reduces

Table 4: ANOVA test results for microhardness of the deposit.

Source	Sum of squares (SS)	Degree of freedom	Mean square	F value	P value (prob > F)	Whether significant or not
Model	$3.334E+005$	14	23817.52	27.17	<0.0001	Significant
P	41417.04	1	41417.04	47.65	<0.0001	
F	$1.226E+005$	1	$1.226E+5$	129.73	<0.0001	
T	1751.04	1	1751.04	4.76	0.0118	
D	7245.38	1	7245.38	8.46	<0.0001	
PF	12265.56	1	12265.56	10.09	<0.0001	
PT	23485.56	1	23485.56	32.46	<0.0001	
PD	1580.06	1	1580.06	1.09	0.0157	
FT	6201.56	1	6201.56	3.00	<0.0001	
FD	14220.56	1	14220.56	15.47	<0.0001	
TD	10251.56	1	10251.56	11.07	<0.0001	
P^2	33380.36	1	33380.36	45.15	<0.0001	
F^2	36063.57	1	36063.57	51.57	<0.0001	
T^2	2480.86	1	2480.86	1.94	0.0039	
D^2	48696.50	1	48696.50	51.89	<0.0001	
Residual	3195.42	15	213.03			
Lack of fit	2608.08	10	260.81	1.51	0.1959	Not significant
Pure error	587.33	5	117.47	Pred. R^2	0.9529	
Cor total	$3.366E+005$	29		Press	15868.32	
Std.deviation	14.60			Mean	671.10	
R^2	0.9905			C.V %	2.17	
Adj. R^2	0.9816			Adeq. Precision	34.478	

Table 5: ANOVA test results for weight loss of the deposit.

Source	Sum of squares	Degree of freedom	Mean square	F value	P value (prob > F)	Whether significant or not
Model	968.18	14	69.16	140.87	<0.0001	Significant
P	40.30	1	40.30	82.74	<0.0001	
F	444.62	1	444.62	905.69	<0.0001	
T	0.35	1	0.35	10.52	0.0048	
D	24.60	1	24.60	50.76	<0.0001	
PF	25.25	1	25.25	51.80	<0.0001	
PT	341.33	1	341.33	695.82	<0.0001	
PD	5.18	1	5.18	10.40	0.0057	
FT	1.76	1	1.76	3.49	0.0814	
FD	50.77	1	50.77	103.27	<0.0001	
TD	31.64	1	31.64	64.30	<0.0001	
P^2	1.28	1	1.28	3.14	0.0968	
F^2	0.077	1	0.077	0.35	0.0519	
T^2	0.75	1	0.75	0.016	0.0418	
D^2	0.26	1	0.26	0.28	0.6044	
Residual	8.77	15	0.58			
Lack of fit	7.73	10	0.77	2.73	0.1399	Not significant
Pure error	1.05	5	0.21	Pred. R^2	0.9616	
Cor total	976.95	29		Press	46.01	
Std.deviation	0.76			Mean	28.39	
R^2	0.9910			C.V %	2.69	
Adj. R^2	0.9826			Adeq. Precision	45.511	

dilution. Less dilution means less hardness. Because more heat is used to melt the powder and less heat melts the substrate, increasing F (constant P, T, D) decreases dilution and increases hardness. Increasing T (constant P, F, D) reduces powder density per square area (g/mm^2), increasing dilution rate and decreasing hardness. Hardness increases when D (constant P, F, T) decreases. Increasing the defocusing distance reduces the energy density per unit of clad pass available, reducing penetration depth and dilution. That is the greatest hardness and the lowest weight loss. Their use in predicting response (hardness and weight loss) in any zone of the experimental area [22] is recommended. The highest attainable hardness value is 820 HV, as illustrated in Figures 6(a)–6(f). Figures 7(a)–7(f) show the minimal weight loss value of 16.31 mg. The settings for maximum hardness and minimal weight loss are 1314 W power,

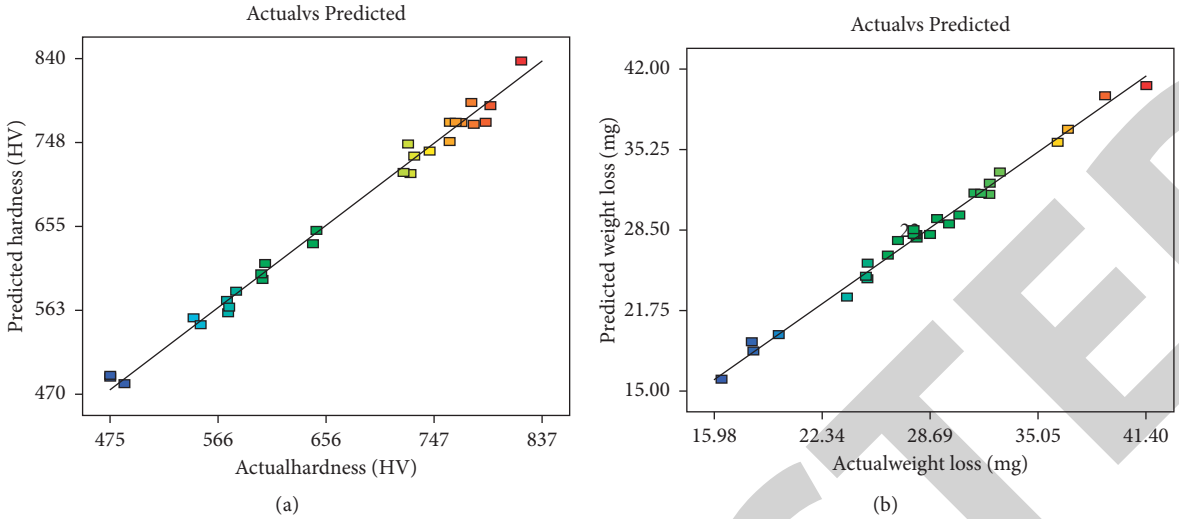

Figure 2: Correlation graphs. (a) Microhardness of deposit. (b) Weight loss of deposit.

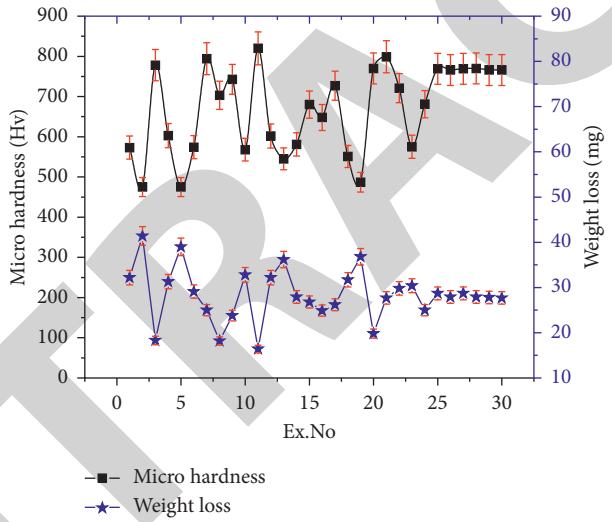

Figure 3: Microhardness and weight loss with error bar for all thirty experiments.

Table 6: Verification results for microhardness.

Sl. No	Power (W)	Powder feed rate (g/min)	Travel speed (mm/min)	Defocusing distance (mm)	Actual hardness (HV)	Predicted hardness (HV)	Error (%)
01	1386	8.5	353	30	815	828	2.7
02	1414	9	437	25	809	821	1.4
03	1329	9	361	32	820	829	1

Table 7: Verification results for wear test weight loss.

Sl. No	Power (W)	Powder feed rate (g/min)	Travel speed (mm/min)	Defocusing distance (mm)	Actual weight loss (mg)	Predicted weight loss (mg)	Error (%)
01	1100	4	325	20	30.7	29.6	3.58
02	1400	6	400	26	29.28	30	−2.45
03	1800	8	470	30	28.02	27.15	3.10

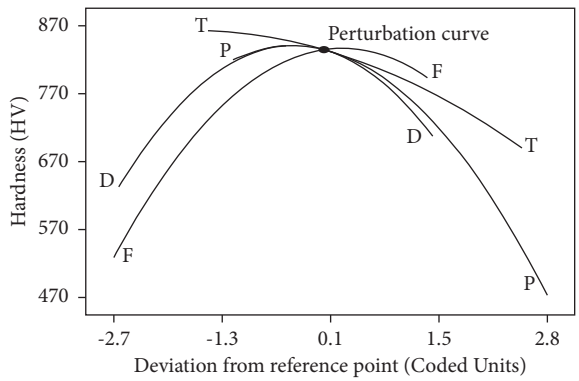

Figure 4: Effect of laser hardfacing processes parameters on hardness.

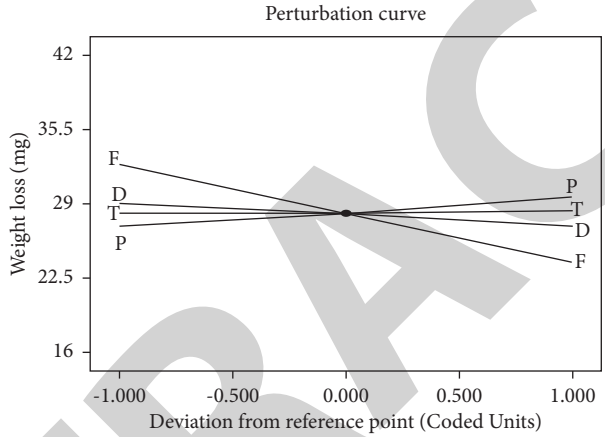

Figure 5: Effect of laser hardfacing processes parameters on weight loss.

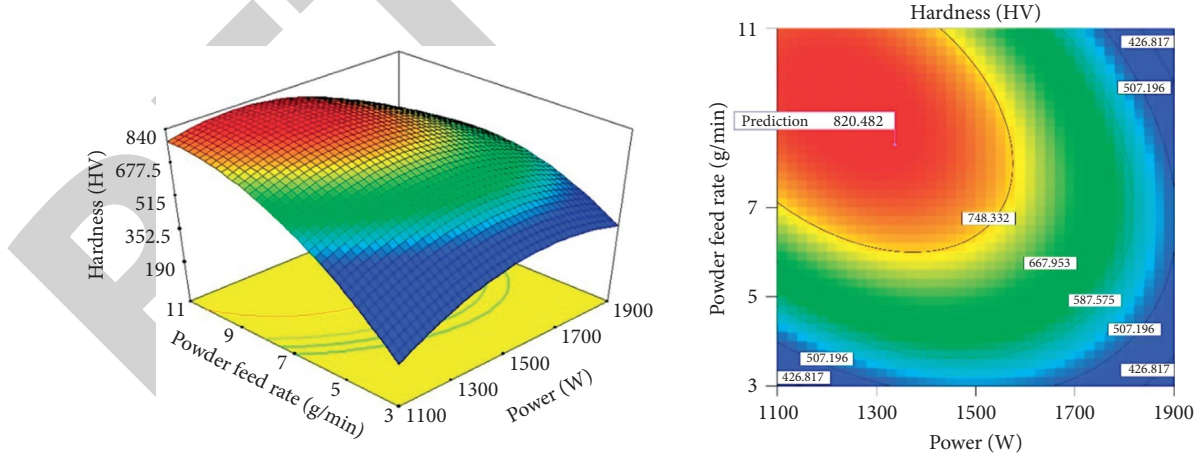

(a)

Figure 6: Continued.

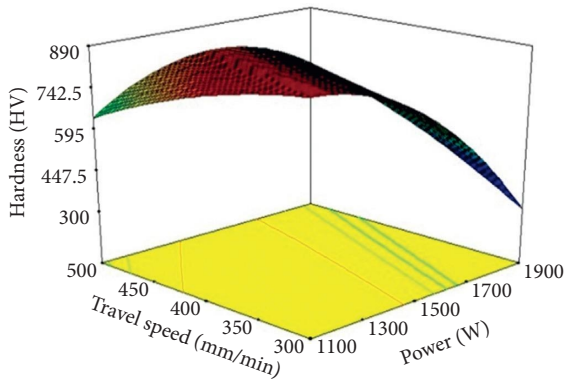

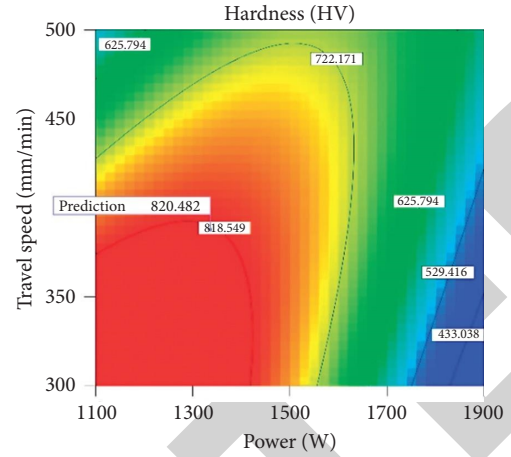

(b)

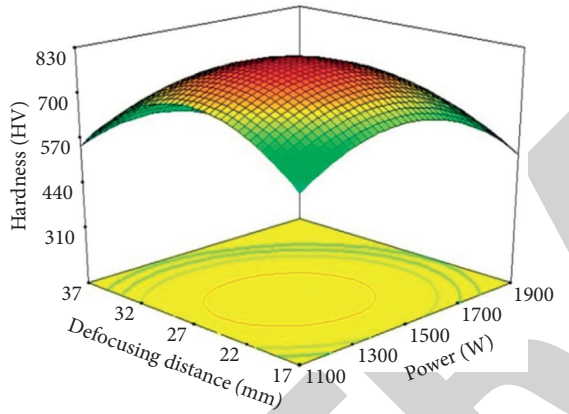

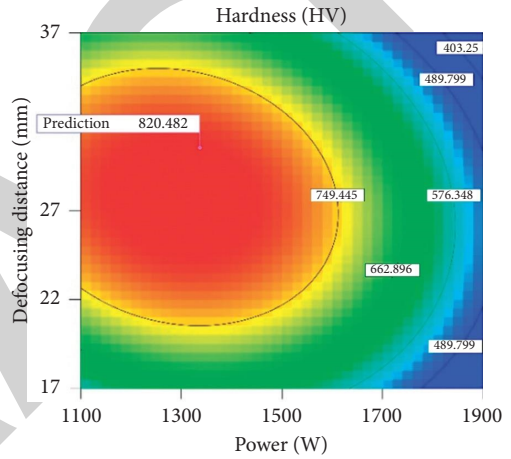

(c)

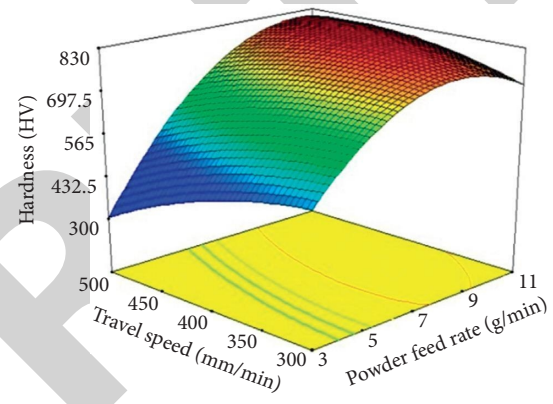

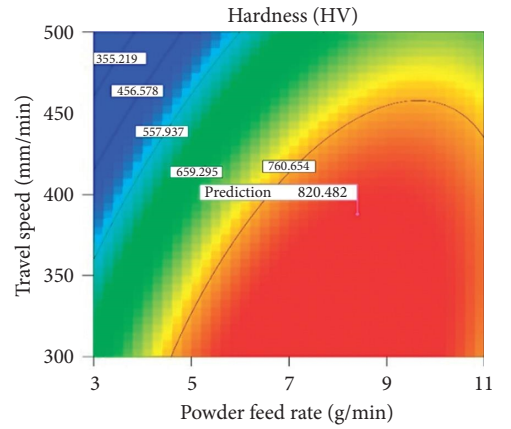

(d)

Figure 6: Continued.

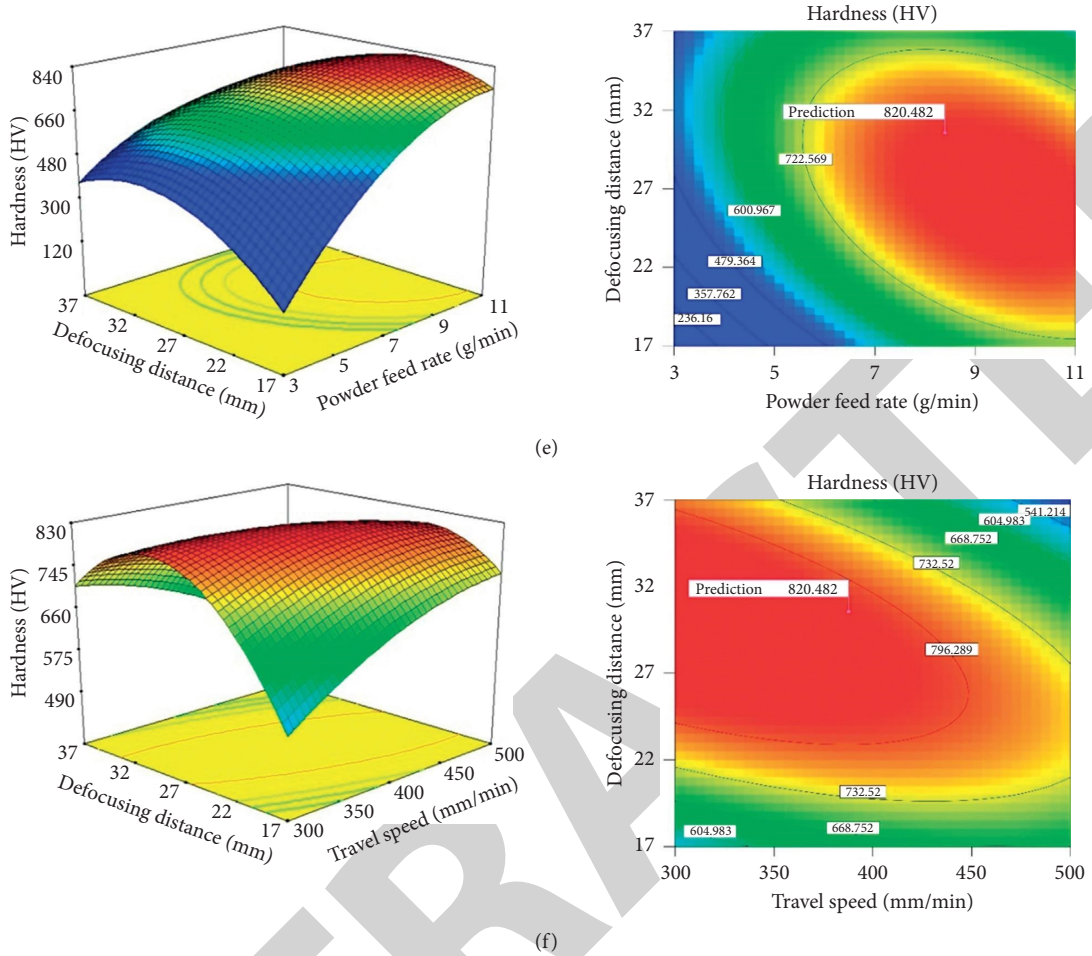

Figure 6: Response surface graphs and contour plots. The interaction between (a) laser power and powder feed rate, (b) laser power and travel speed, (c) laser power and defocusing distance, (d) powder feed rate and travel speed, (e) powder feed rate and defocusing distance, and (f) travel speed and defocusing distance is examined.

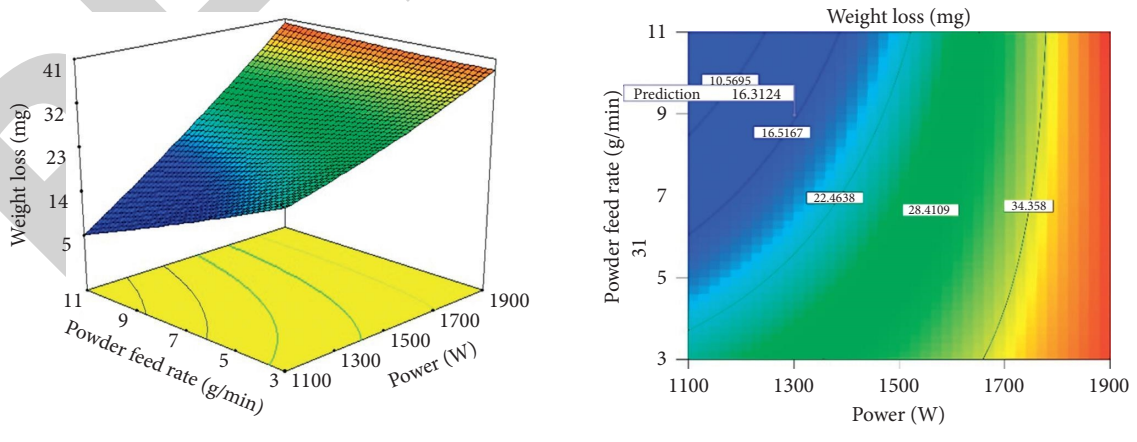

(a)

Figure 7: Continued.

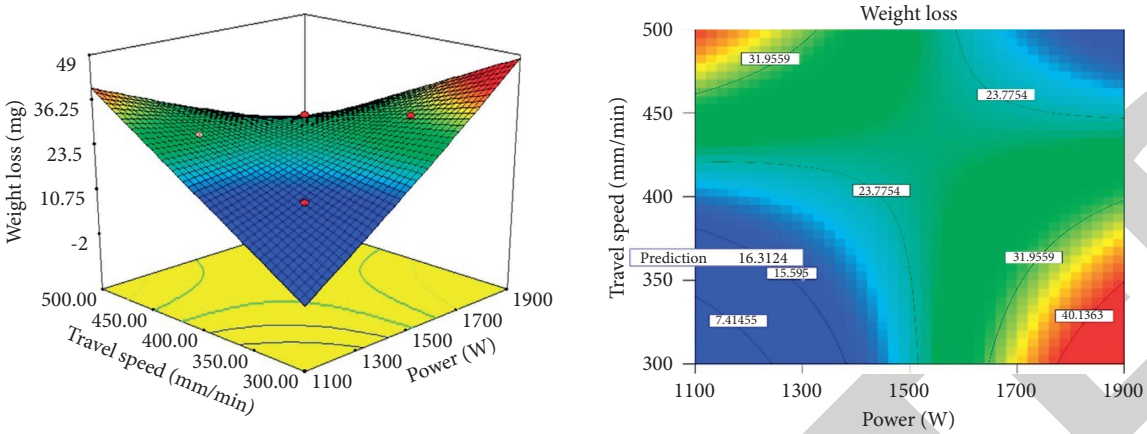

(b)

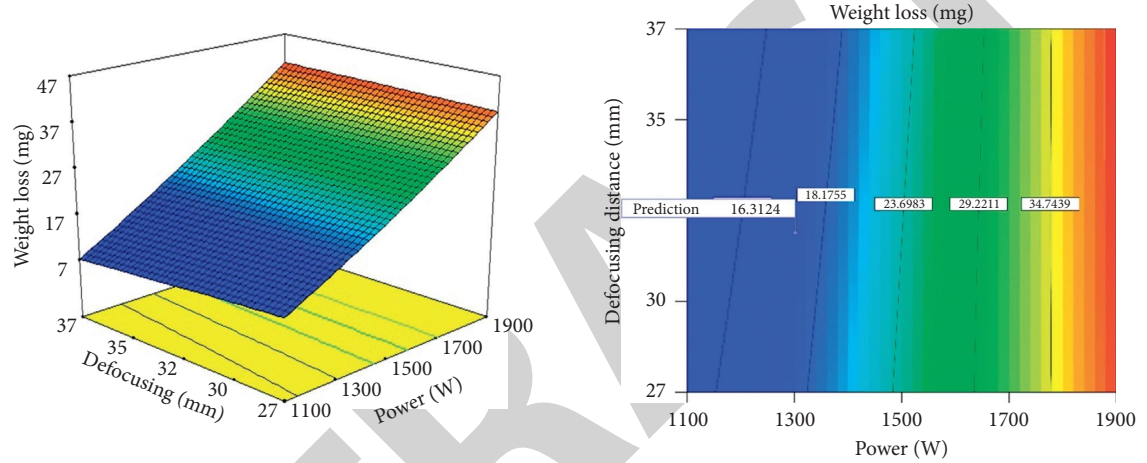

(c)

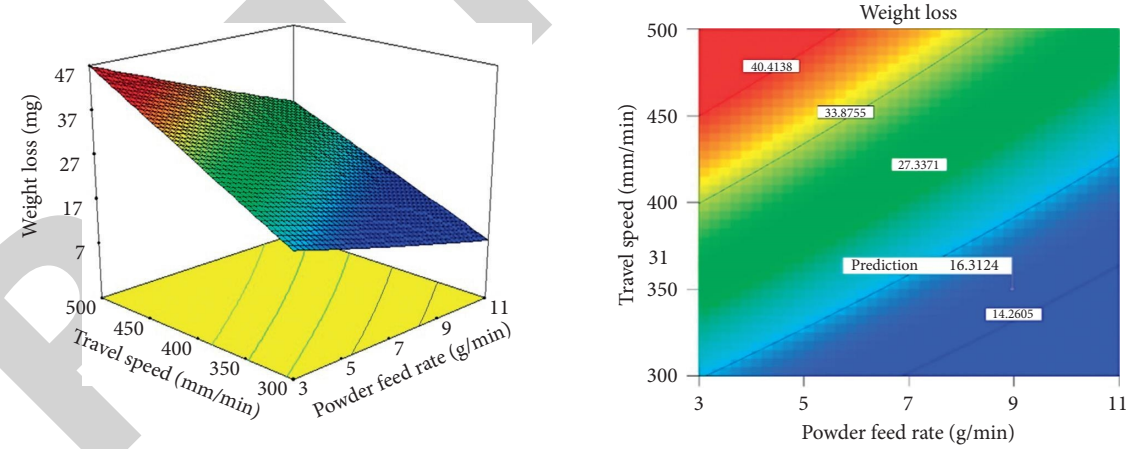

(d)

Figure 7: Continued.

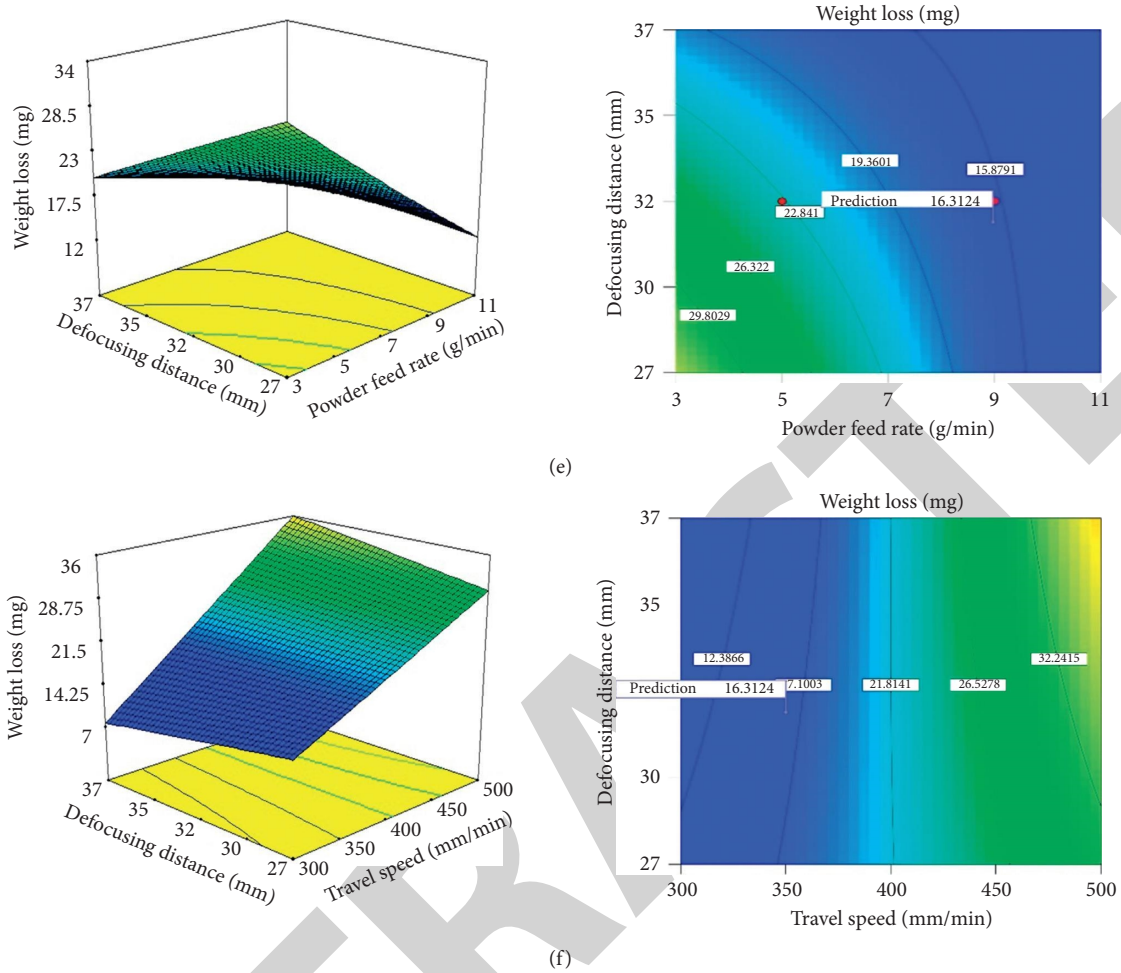

Figure 7: Response surface graphs and contour plots. The interaction between (a) laser power and powder feed rate, (b) laser power and travel speed, (c) laser power and defocusing distance, (d) powder feed rate and travel speed, (e) powder feed rate and defocusing distance, and (f) travel speed and defocusing distance is examined.

9 g/min powder feed, 366 mm/s travel speed, and 32 mm defocusing distance. There is a more important process parameter with a higher F ratio.

Using the F ratio, it can be inferred that the powder feed rate is the most important element in exploiting hardness, followed by power, defocusing distance, and travel speed [23]. To verify the empirical relationship's prediction abilities, three additional confirmation tests were run using hardfacing process parameters selected at random from the practical working range (Table 8). The actual answer was the mean of three findings. The produced findings show the empirical connection is accurate with a 5% variance. Table 9 lists optimized laser hardfacing parameters.

3.3. Graphical Optimization for Deposit Desired Quality Characteristics. Numerous responses are handled graphically by superimposing significant response contours on a contour map. Then, a visual search may provide the most accurate results. When confronted with a large number of answers, it is preferable to begin with numerical optimization in order to identify a viable area. The graphical optimization procedure included the numerical optimization criteria, and the lower and upper bounds were determined using the numerical optimization findings. Overlay plots may be used to rapidly determine the values of the laser hardfacing process parameters required to obtain the desired response value for this kind of material [24, 25].

Given that deposit hardness is directly related to wear resistance (weight loss), linking microhardness and wear resistance is critical. Hardness improves wear resistance and therefore reduces weight loss. Deposit resistance typically reflects hardness. This leads to the study of microhardness and wear resistance combined [26–28]. Given the above, it is preferable to run a graphical optimization result and let the visual inspection choose the best deposit condition. The overlay plot's shaded regions do not meet the proposed criteria. Figure 8 shows the graphical optimization charts. To find the desired response within the design space, one can use this overlay plot. An optimization study finds optimal spraying conditions to achieve desired microstructural and mechanical properties [29-33].

Table 8: Validation test results for the developed empirical relationship.

S. no.	Power (W)	Powder feed rate (g/min)	Travel speed (mm/min)	Defocusing distance (mm)	Actual hardness (HV)	Predicted hardness (HV)	Error (%)
01	1400	4	325	20	585	570	−2.6
02	1600	6	375	24	658	635	−3.6
03	1800	10	450	35	783	797	1.7

Table 9: Optimal parameters for laser hardfacing.

S. no.	Main parameters	
1	Laser power (W)	1300
2	Traverse speed (mm/min)	350
3	Powder feed rate (grams/min)	9
4	Defocusing distance (mm)	32

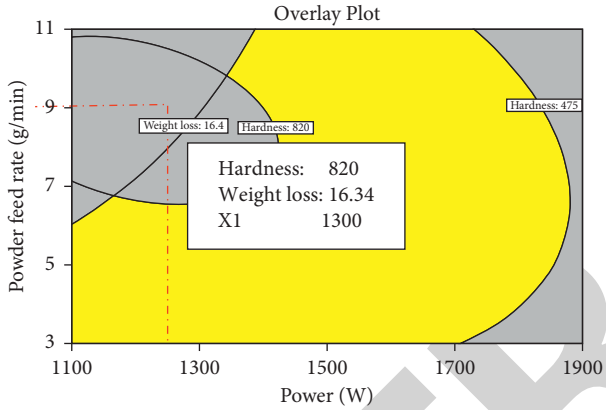

Figure 8: Graphical optimization plot shows the response of optimized process parameters for minimum weight loss and maximum hardness.

4. Conclusions

(1) An empirical relationship was developed to predict the hardness of nickel-based layer deposited on 316LN austenitic stainless steel substrate with 95% confidence level by incorporating important laser hardfacing parameters

(2) The laser hardfacing parameters (power, powder feed rate, travel speed, defocusing distance) were optimized for Ni-based deposit, by adopting multi-response optimization with the RSM approach. However, the illustrated approach and the methodology of the response surfaces are universal and can be applied for any specific application to tailor the deposit properties

(3) A maximum hardness of 820 HV and minimum weight loss of 16.31 mg could be achieved in the deposit made using laser power of 1314 W, powder feed rate of 9 g/min, a travel speed of 366 mm/min, and defocusing distance of 32 mm

(4) Of the four laser hardfacing parameters, the powder feed rate (based on F value) is the major influencing factor to predict the hardness followed by power, travel speed, and defocusing distance [31–33]

Data Availability

The data used to support the findings of this study are included within the article.

Conflicts of Interest

The authors declare that they have no conflicts of interest.

Acknowledgments

The authors thank the UGC-DAE Consortium for giving financial support in order to conduct this research (Project No. CSR-KN/CRS-56/2013-14/656, dated 04.09.13). The authors would like to convey their heartfelt gratitude to M/s. Geometrix Laser Solutions Pvt Limited, Tada, for providing them with laser hardfacing services. The authors would also like to express their heartfelt gratitude to the Director, IGCAR, Kalpakkam, for providing the basic metal.

References

[1] L. C. Lim, Q. Ming, and Z. D. Chen, "Microstructures of laser-clad nickel-based hardfacing alloys," *Surface and Coatings Technology*, vol. 106, no. 2-3, pp. 183–192, 1998.

[2] A. K. Bhaduri, R. Indira, S. K. Albert, B. P. S. Rao, S. C. Jain, and S. Asokkumar, "Selection of hardfacing material for components of the Indian prototype fast breeder reactor," *Journal of Nuclear Materials*, vol. 334, no. 2-3, pp. 109–114, 2004, Frenk and W. Kurz: Mater. Sci. Eng. A, 1993, vol. 173, pp. 339–342.

[3] S. L. Mannan, C. S. C. B. Raj, and S. B. Bhoje, *Materials R&D for Prototype Fast Breeder Reactor*, S. L. Mannan and M. D. Mathew, Eds., Indira Gandhi Centre for Atomic Research, Kalpakkam, 2003.

[4] G. Chakraborty, S. K. Albert, and A. K. Bhaduri, "Effect of dilution and cooling rate on microstructure and magnetic properties of Ni base hardfacing alloy deposited on austenitic stainless steel," *Materials Science and Technology*, vol. 28, no. 2, pp. 454–459, 2012.

[5] N. Jeyaprakash and C.-H. Yang, "Comparative study of NiCrFeMoNb/FeCrMoVC laser cladding process on nickel-based superalloy," *Materials and Manufacturing Processes*, vol. 35, no. 12, pp. 1383–1391, 2020.

[6] N. Jeyaprakash, CH. Yang, M. Duraiselvam, Muthukannan, and S. Sivasankaran, "Comparative study of laser melting and pre-placed Ni–20% Cr alloying over nodular iron surface," *Archiv.Civ.Mech.Eng*, vol. 20, no. 20, p. 0030, 2020.

[7] N. Jeyaprakash, C.-H. Yang, S. Sivasankaran, and S. Sivasankaran, "Formation of FeCrMoVC layers on AA6061 by laser cladding process: microstructure and wear

characteristics," *Transactions of the Indian Institute of Metals*, vol. 73, no. 6, pp. 1611–1617, 2020.

[8] D. Zhang and X. Zhang, "Laser cladding of stainless steel with Ni-Cr3C2 and Ni-WC for improving erosive-corrosive wear performance," *Surface and Coatings Technology*, vol. 190, no. 2-3, pp. 212–217, 2005.

[9] L. J. da Silva and A. S. C. M. D'Oliveira, "NiCrSiBC coatings: Effect of dilution on microstructure and high temperature tribological behavior," *Wear*, vol. 350-351, pp. 130–140, 2016.

[10] S. K. Albert, S. Venkadesan, and S. L. Mannan, "Studies on a nickel base hardfacing alloy deposited on stainless steel," in *Proceedings of the Symp. On "Joining of materials for 2000 AD"*, pp. 363–369, Indian Institute of Welding, Tiruchirapalli, India, December 1991.

[11] D. K. Dwivedi, "Adhesive wear behaviour of cast aluminium-silicon alloys: overview," *Materials & Design (1980-2015)*, vol. 31, no. 5, pp. 2517–2531, 2010.

[12] K. Gurumoorthy, M. Kamaraj, K. P. Rao, A. S. Rao, and S. Venugopal, "Microstructural aspects of plasma transferred arc surfaced Ni-based hardfacing alloy," *Materials Science and Engineering: A*, vol. 456, no. 1-2, pp. 11–19, 2007.

[13] I. Hemmati, V. Ocelík, and J. T. M. De Hosson, "Dilution effects in laser cladding of Ni-Cr-B-Si-C hardfacing alloys," *Materials Letters*, vol. 84, pp. 69–72, 2012.

[14] Astm G. 99 – 04, *Standard Test Method for Wear Testing with a Pin-On-Disk Apparatus*, ASTM International, West Conshohocken, PA, 2016, https://www.astm.org.

[15] I. Hemmati, *Laser-deposited metallic coatings: processing, characterization, alloy development*, Ph.D Thesis, University of Groningen, Groningen, Netherlands, 2013.

[16] D.-G. Ahn, "Hardfacing technologies for improvement of wear characteristics of hot working tools: a Review," *International Journal of Precision Engineering and Manufacturing*, vol. 14, no. 7, pp. 1271–1283, 2013.

[17] S. J. S. Chelladurai, K. Murugan, A. P. Ray, M. Upadhyaya, V. Narasimharaj, and S. Gnanasekaran, "Optimization of process parameters using response surface methodology: a review," *Materials Today: Proceedings*, vol. 37, no. 2, pp. 1301–1304, 2021.

[18] Q. Ming, L. C. Lim, and Z. D. Chen, "Laser cladding of nickel-based hardfacing alloys," *Surface and Coatings Technology*, vol. 106, no. 2-3, pp. 174–182, 1998.

[19] H. Zhang, Y. Shi, M. Kutsuna, and G. J. Xu, "Laser cladding of Colmonoy 6 powder on AISI316L austenitic stainless steel," *Nuclear Engineering and Design*, vol. 240, no. 10, pp. 2691–2696, 2010.

[20] D. C. Montgomery, *Design and Analysis of Experiments*, Wiley, Hoboken, New Jersey, 2004.

[21] M. Qian, L. C. Lim, Z. D. Chen, and W. I. Chen, "Parametric studies of laser cladding processes," *Journal of Materials Processing Technology*, vol. 63, no. 1–3, pp. 590–593, 1997.

[22] A. I. Khuri and J. A. Cornell, *Response Surfaces: Designs and Analyses*, CRC Press, Boca Raton, Florida, Second Edition, 1996.

[23] K. Y. Benyounis and A. G. Olabi, "Optimization of different welding processes using statistical and numerical approaches - a reference guide," *Advances in Engineering Software*, vol. 39, no. 6, pp. 483–496, 2008.

[24] C.-L. Tien and S.-W. Lin, "Optimization of process parameters of titanium dioxide films by response surfaces methodology," *Optics Communications*, vol. 266, no. 2, pp. 574–581, 2006.

[25] S. Gnanasekaran, S. Senthil Kumar, N. raj Venugopal et al., "Effect of laser power on microstructure and tensile properties of pulsed Nd:YAG laser beam welded AISI 301 austenitic stainless steel joints," *Materials Today: Proceedings*, vol. 37, pp. 934–939, 2020.

[26] S. Gnanasekaran, G. Padmanaban, V. Balasubramanian, H. Kumar, and S. K. Albert, "Correlation between travel speed, microstructure, mechanical properties and wear characteristics of Ni-based hardfaced deposits over 316LN austenitic stainless steel," *High Temperature Materials and Processes*, vol. 38, no. 2019, pp. 16–29, 2019.

[27] G. S. G. Padmanaban, V. Balasubramanian, and S. K. Albert, "Laser hardfacing of colmonoy-5 (Ni-Cr-Si-B-C) powder onto 316LN austenitic stainless steel: effect of powder feed rate on microstructure," *Mechanical Properties and Tribological Behavior" Lasers in Engineering*, vol. 42, no. 4-6, pp. 283–302, 2019.

[28] G. Padmanaban and V. Balasubramanian, "Optimization of laser beam welding process parameters to attain maximum tensile strength in AZ31B magnesium alloy," *Optics & Laser Technology*, vol. 42, no. 8, pp. 1253–1260, 2010.

[29] J. D. Majumdar and I. Manna, *Laser-Assisted Fabrication of Materials*, Indranil, Ed., vol. 171, Springer, Berlin, Germany, 2012, Series in Materials Science.

[30] D. Kesavan and M. Kamaraj, "The microstructure and high temperature wear performance of a nickel base hardfaced coating," *Surface and Coatings Technology*, vol. 204, no. 24, pp. 4034–4043, 2010.

[31] S. Gnanasekaran, G. Padmanaban, V. Balasubramanian, H. Kumar, and S. K. Albert, "Optimizing the laser parameters to attain maximum hardness in nickel based hardfacing surfaces," *Journal of the Mechanical Behavior of Materials*, vol. 26, no. 2-3, pp. 113–126, 2017.

[32] S. Gnanasekaran, G. Padmanaban, and V. Balasubramanian, "Effect of laser power on metallurgical, mechanical and tribological characteristics of hardfaced surfaces of nickel-based alloy," *Lasers in Manufacturing and Materials Processing*, vol. 4, no. 4, pp. 178–192, 2017.

[33] S. Gnanasekaran, G. Padmanaban, and V. Balasubramanian, "Effect of laser hardfacing process parameters on microstructural characteristics and microhardness of Ni-Cr-B-Si-C deposit on austenitic stainless steel substrate," *Journal of Advanced Microscopy Research*, vol. 12, no. 3, pp. 173–181, 2017.